Supplement to: Aerosol loading delays droplet activation and suppresses drizzle mode Ka-band radar signatures in LES–LCM simulations of shallow cumulus clouds

Junghwa Lee[1,2], Patric Seifert[1], Tempei Hashino[3], and Yign Noh[4]

[1]Leibniz Institute for Tropospheric Research (TROPOS), Leipzig, Germany
[2]High-Performance Computing Center Stuttgart (HLRS), University of Stuttgart, Stuttgart, Germany
[3]Kochi University of Technology, Kami, Japan
[4]Yonsei University, Seoul, Republic of Korea

Supplementary Figures

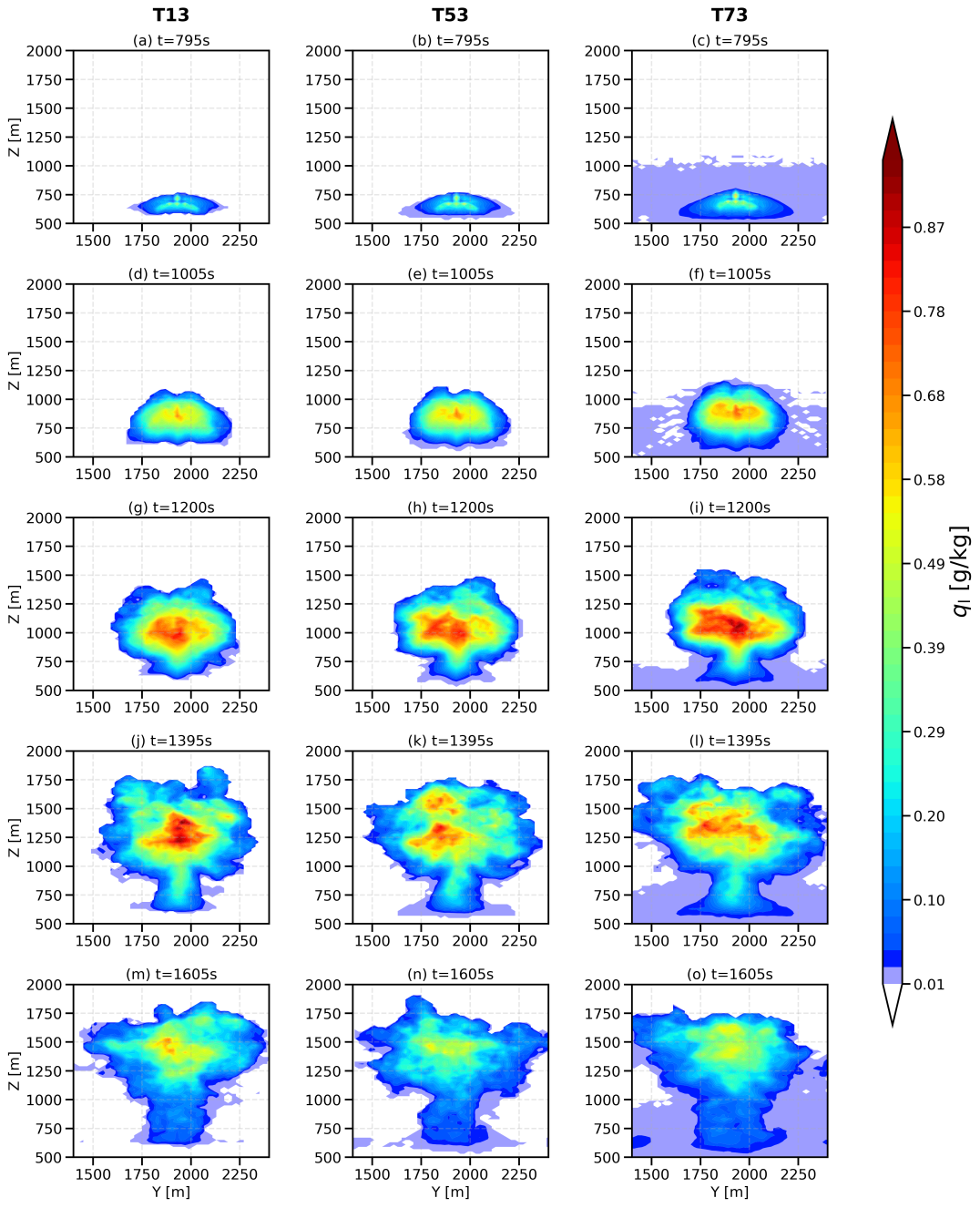

Figure S1. Time evolution of cloud liquid water mixing ratio q_l in Y–Z cross-sections for T13, T53, and T73 at approximately 800, 1000, 1200, 1400, and 1600 s. The spatial organization and vertical extent of condensate differ systematically with aerosol loading.

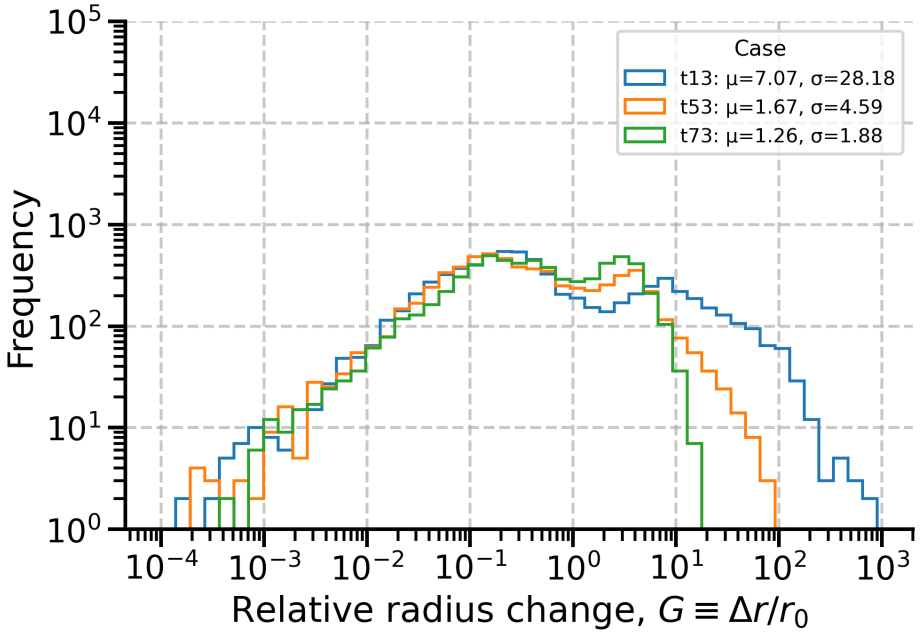

Figure S2. Distribution of the relative radius change $G \equiv \Delta r/r_0$ for T13, T53, and T73. Higher aerosol loading shifts the distribution toward smaller G values, indicating reduced spectral broadening and fewer rapid-growth trajectories.

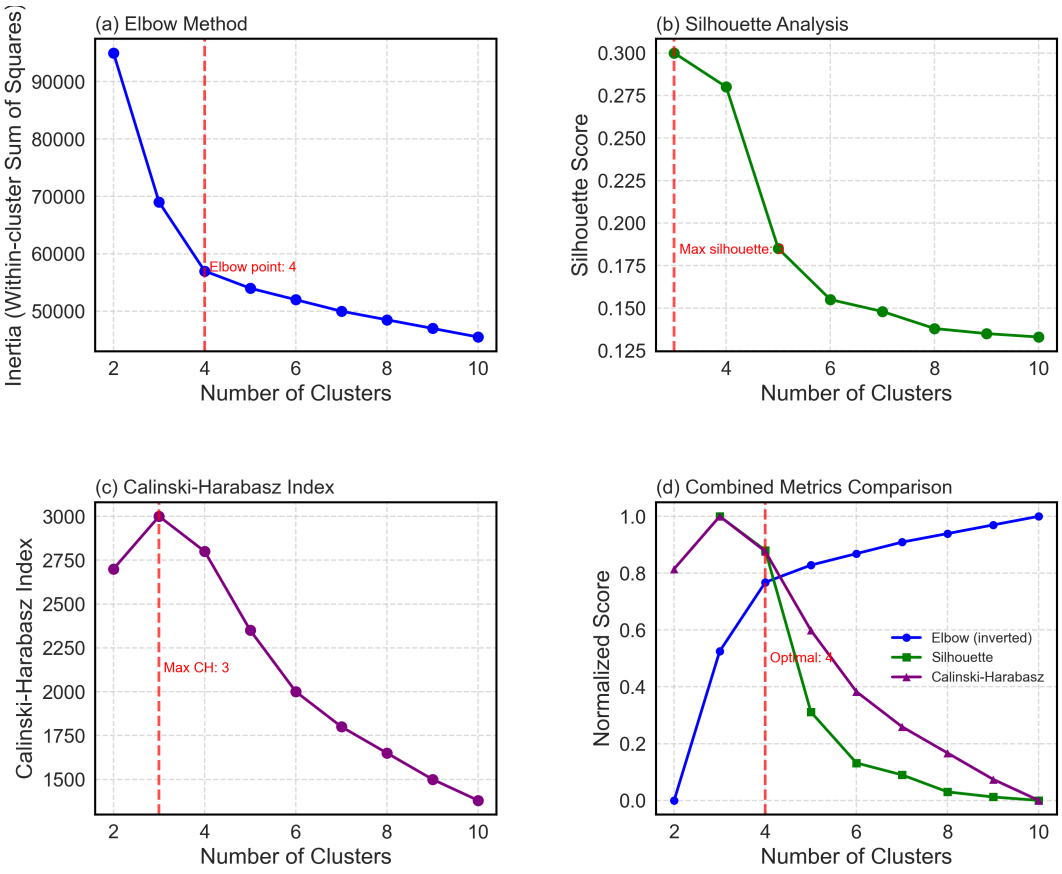

Figure S3. Cluster optimization diagnostics for the RH-history-based trajectory clustering. Panels show the elbow heuristic (Thorndike, 1953), silhouette analysis (Rousseeuw, 1987), and the Calinski–Harabasz index (Calinski and Harabasz, 1974), together with a normalized combined comparison. The elbow curve favors $k = 4$, whereas the silhouette and Calinski–Harabasz scores peak at $k = 3$. In the combined view, $k = 4$ is adopted as the compromise choice used in the main text.

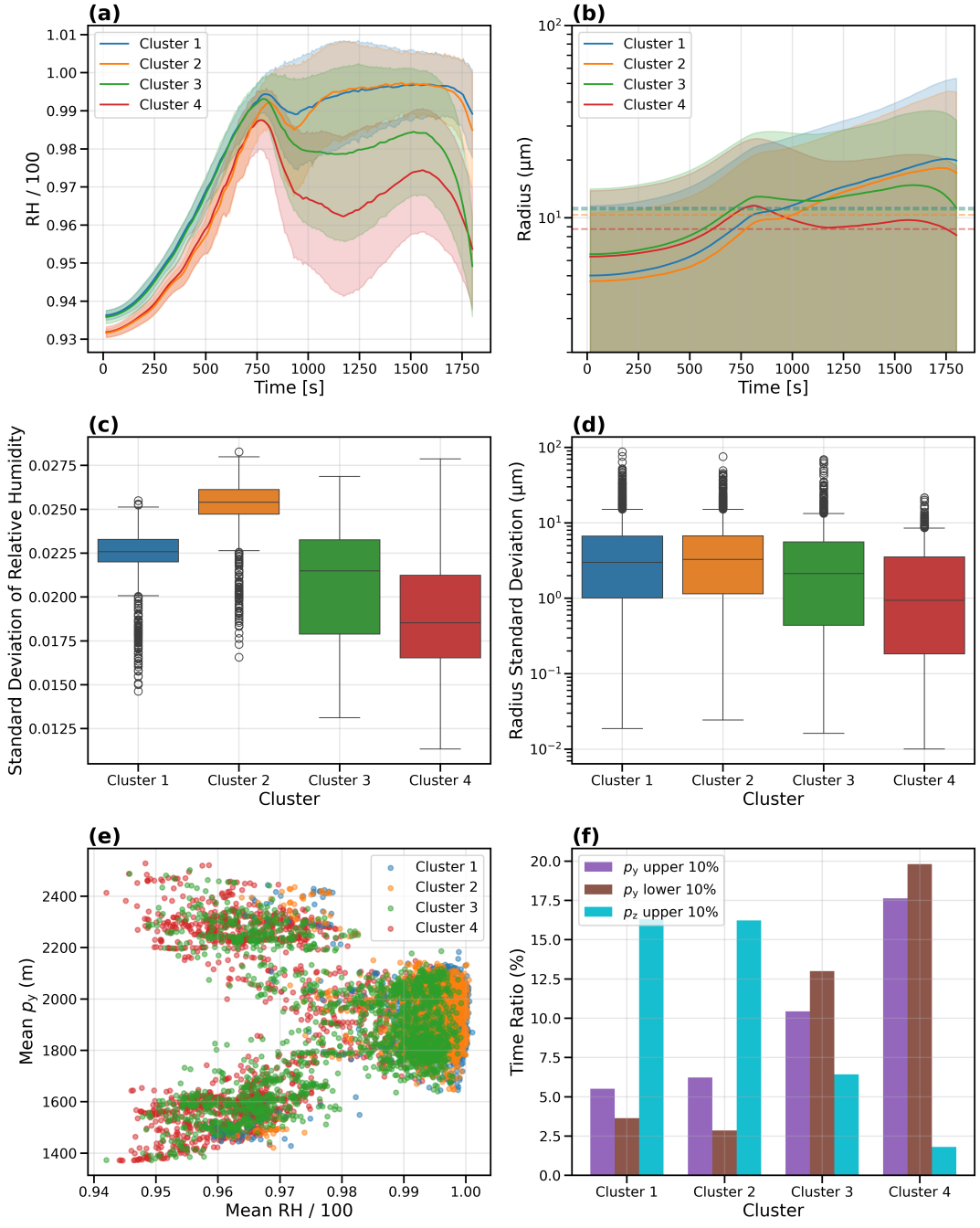

Figure S4. As Fig. 3 in the main text but for the polluted case T73. Peak RH excursions are reduced and radius variability is narrower compared to T13. Saturation corresponds to RH = 1.

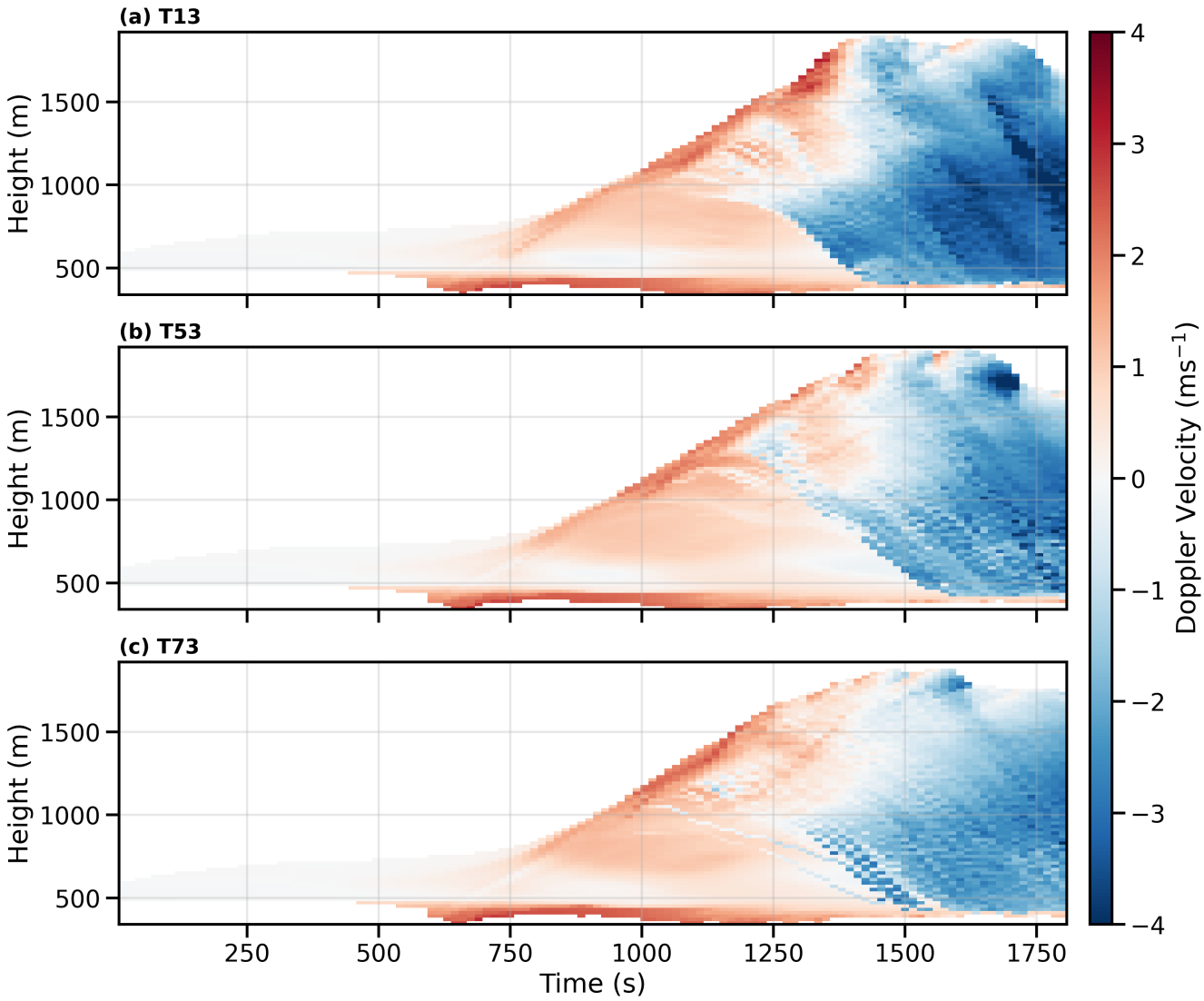

Figure S5. Time–height plots of mean Doppler velocity V_{D} for T13, T53, and T73. Positive values indicate upward motion. The magnitude and structure of downdrafts associated with precipitation differ with aerosol loading.

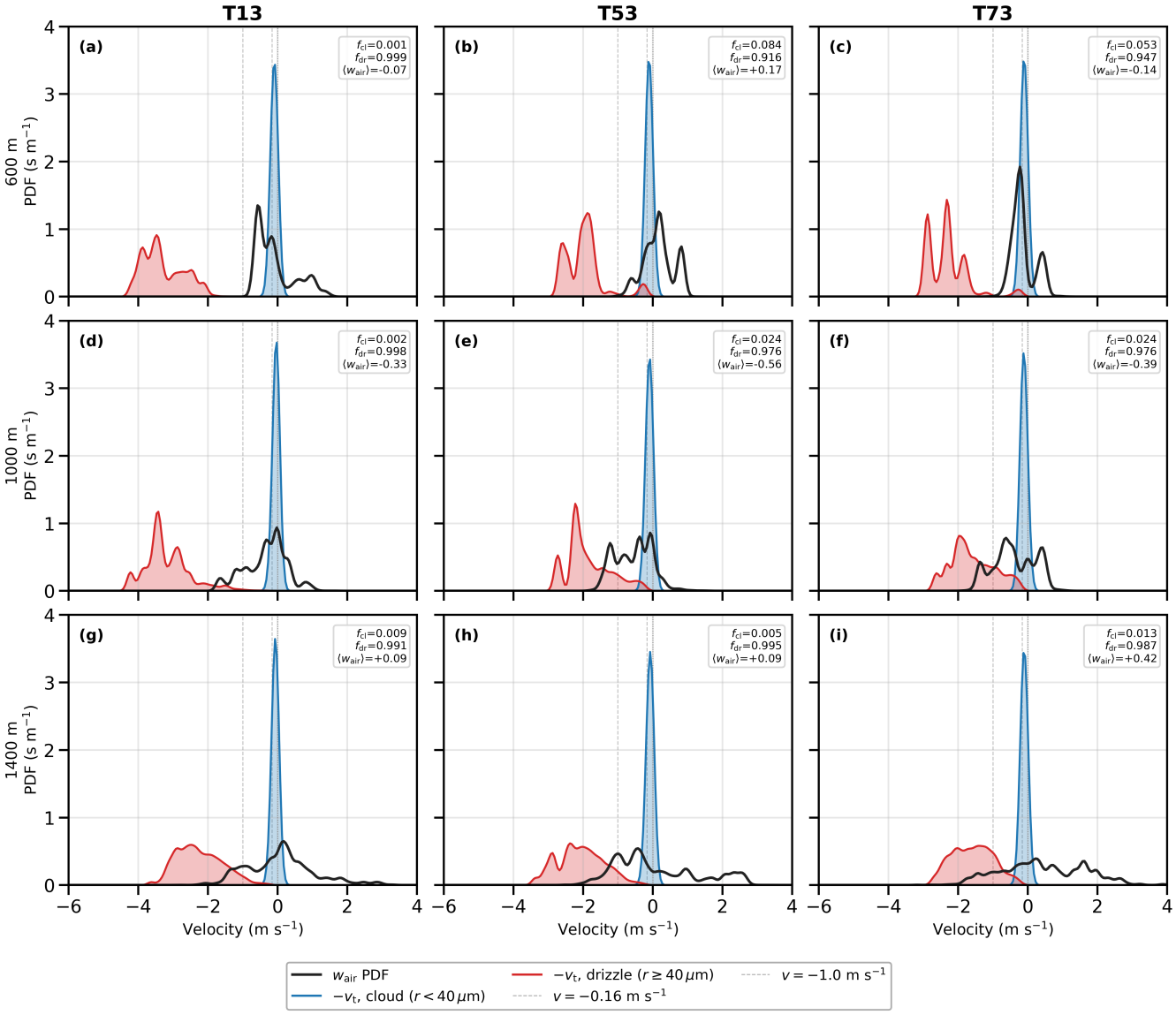

Figure S6. Reflectivity-weighted ($W \cdot r^6$) probability density functions of the resolved air vertical velocity w_{air} (black, positive upward), of the cloud-mode terminal fall velocity $-v_{\mathrm{t}}$ for $r < 40\,\mu\mathrm{m}$ (blue), and of the drizzle-mode terminal fall velocity $-v_{\mathrm{t}}$ for $r \geq 40\,\mu\mathrm{m}$ (red), at $t = 1600\,\mathrm{s}$. Columns correspond to T13, T53, and T73. Rows correspond to $z = 600\,\mathrm{m}$, $1000\,\mathrm{m}$, and $1400\,\mathrm{m}$. Vertical dashed lines mark $v = -0.16\,\mathrm{m\,s^{-1}}$, the terminal velocity of a $r = 40\,\mu\mathrm{m}$ droplet at the cloud–drizzle threshold, and $v = -1.0\,\mathrm{m\,s^{-1}}$, taken as a reference for sedimentation-dominated fall. Inset values report the reflectivity fractions contributed by the cloud and drizzle modes (f_{c} and f_{d}) and the mean resolved vertical velocity $\langle w_{\mathrm{air}} \rangle$ in $\mathrm{m\,s^{-1}}$. Sampling follows Fig. 9 in the main text.

References

Calinski, T. and Harabasz, J.: A dendrite method for cluster analysis, Communications in Statistics, 3, 1–27, https://doi.org/10.1080/03610927408827101, 1974.

Rousseeuw, P. J.: Silhouettes: A graphical aid to the interpretation and validation of cluster analysis, Journal of Computational and Applied Mathematics, 20, 53–65, https://doi.org/10.1016/0377-0427(87)90125-7, 1987.

Thorndike, R. L.: Who Belongs in the Family?, Psychometrika, 18, 267–276, https://doi.org/10.1007/BF02289263, 1953.